Real-time optical monitoring of the heteroepitaxy of oxides by an oblique-incidence reflectance difference technique

Fan Chen, Huibin Lu, Tong Zhao, Kui-juan Jin, Zhenghao Chen, and Guozhen Yang*

Laboratory of Optical Physics, Institute of Physics, Center for Condensed Matter Physics, Chinese Academy of Sciences, P.O. Box 603, Beijing 100080, People's Republic of China

(Received 21 July 1999; revised manuscript received 5 November 1999)

Monolayer oscillations and interference oscillations were observed during the interrupted heteroepitaxy of Nb-doped strontium titanate on $SrTiO_3$ by an oblique-incidence reflectance difference (OIRD) technique. The optical monolayer oscillations were verified by simultaneously monitored reflection high-energy electron diffraction. In modeling the surface structure as a four-layer stack, we consider the outermost incomplete layer as two parts, a homogeneous isotropic media layer with an average dielectric constant and a film layer below that with the dielectric constant of the bulk film. The numerical simulation of a simple deposition process and Monte Carlo simulation are carried out to reproduce the OIRD interference oscillations and monolayer response, respectively. The simulated amplitude of the monolayer oscillations is in good agreement with the experimental results.

INTRODUCTION

Real-time monitoring of the layer-by-layer growth of thin films has become an essential part of thin-film sciences and techniques. Optical diagnostic techniques have the advantages of being noninvasive, nondestructive, and can be used in many transparent ambients over conventional reflection high-energy electron diffraction (RHEED). During the last few decades, optical methods such as spectral ellipsometry,[1] reflectance difference spectroscopy (RDS),[2–4] *p*-polarized reflection spectroscopy (PRS),[5,6] and laser light scattering,[7] have demonstrated their abilities in monitoring film thickness, optical properties, chemical composition, and surface structures. RDS measures the optical anisotropy due to the difference between the reflectance of light polarized along the two principal axes in the surface plane. It is not suitable for the monitoring of those materials that lack in-plane optical anisotropy. PRS measures the reflectivity of *p*-polarized light. The PRS signals mainly come from a surface reaction layer,[5,6] whose chemical composition and structures are different from those of the bulk film. It can be used on pulsed chemical beam epitaxy.[5,6] As in the case of laser ablation or laser molecular-beam epitaxy (laser MBE), where there is not such a surface reaction layer, some problems remain. Recently, a type of reflectance difference technique, oblique-incidence reflectance difference (OIRD), was reported to be used for monitoring the homoepitaxy of $SrTiO_3$.[8] Previous to that, OIRD had been demonstrated to be sensitive to a relative reflectivity change $\Delta R/R = 1\times10^{-5}$ and to a coverage change $\Delta\theta = 0.02$.[9]

In this paper, by using the oblique-incidence reflectance difference method on the heteroepitaxial growth of Nb-doped strontium titanate (Nb:STO) on $SrTiO_3$ (STO), we obtained monolayer OIRD response which is consistent with the RHEED intensity oscillations signal. Interference oscillations between the reflected light from the surface and that from the film/substrate interface have been observed as well. In modeling the surface structure as a four-layer stack, we consider the outermost incomplete layer as two parts, a homogeneous isotropic media layer with an average dielectric constant and a film layer below that with the dielectric constant of the bulk film. Thus, the surface structure can be described as a four-layer stack.[5] The OIRD relative intensity is calculated from the multiple reflection of the probe light by this four-layer stack. The theoretical results obtained by numerical simulations and Monte Carlo simulations are in good agreement with the experimental results. Our work shows that OIRD takes the potentiality of monitoring surface roughness and morphologies and can be taken as a good assistant of RHEED. The study also indicates that further study may make it possible to obtain more information on the processes and the mechanisms of low dimension growth on surfaces.

EXPERIMENTS

The OIRD system is equipped to the vacuum chamber of a laser molecular-beam epitaxy (laser-MBE) system.[10] A standard RHEED apparatus is equipped with its incidence plane coinciding with the [010] axis of the substrate surface and the incidence angle of the electron beam is 87°. The sketch of the optical setup of OIRD is shown in Fig. 1. The initially *p* polarized laser beam from a 4-mW linearly polarized HeNe laser is modulated by a photoelastic modulator

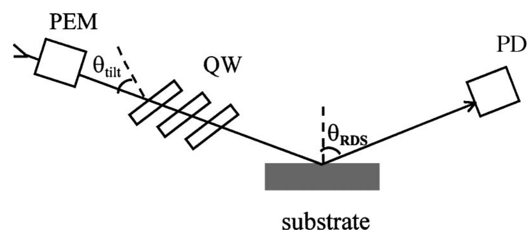

FIG. 1. Sketch of the optical setup of the oblique-incidence reflectance difference (OIRD) measurement. PEM: photoelastic modulator. QW: fused quartz parallel plate. PD: biased silicon photodiode.

 ©2000 The American Physical Society

before impinging to the substrate surface. The p polarization bisects the two principal axes of the modulator, which produces a phase shift between the two components along the principal axes at a frequency of $\Omega = 50\,\text{kHz}$. The maximum phase is set at π or 180°. The three fused quartz plates placed after the modulator with their incidence planes overlapping with that of the substrate are used to change the relative transmittance of the s- and p-polarized component. The incident angle to the substrate surface is $\theta_{\text{RDS}} = 85°$ with the optical incidence plane coinciding with the [100] axis of the substrate surface. The reflected beam intensity is detected by a biased silicon photodiode. The output of the photodiode is transferred to a lock-in amplifier (Stanford Research 510) with its reference frequency at twice that of the modulation frequency. The output $I(2\Omega)$ of the lock-in amplifier is given by[8]

$$I(2\Omega) = \frac{1}{2} J_2(\Phi) I_{inc} [|r_p(\theta_{\text{RDS}}) t_p(\theta_{\text{tilt}})|^2 - |r_s(\theta_{\text{RDS}}) t_s(\theta_{\text{tilt}})|^2], \tag{1}$$

where $r_p(\theta_{\text{RDS}})$ and $r_s(\theta_{\text{RDS}})$ are the reflectance coefficients for p- and s-polarized light at the incidence angle θ_{RDS}, while $t_p(\theta_{\text{tilt}})$ and $t_s(\theta_{\text{tilt}})$ are the total transmission coefficients for p- and s-polarized light through the fused quartz plates at a tilt angle θ_{tilt}, respectively. $J_2(\Phi)$ is the Bessel function of the second kind. More detailed information about the experimental conditions are given elsewhere.[8] One of the key points of this technique is the three plates setting between the modulator and the sample, which adjust the relative intensity of the incident s- and p-polarized light to make a nearly zero background for the initial status. This technique improves the signal-to-noise ratio and the sensitivity by two orders of magnitude. For the initial intensity $I(2\Omega) = 0$, we get

$$|r_{p0}(\theta_{\text{RDS}}) t_p(\theta_{\text{tilt}})|^2 = |r_{s0}(\theta_{\text{RDS}}) t_s(\theta_{\text{tilt}})|^2. \tag{2}$$

Thus the general output intensity comes to

$$I(2\Omega) = \frac{1}{2} J_2(\Phi) I_{inc} |r_{p0}(\theta_{\text{RDS}}) t_p(\theta_{\text{tilt}})|^2 \left[\left| \frac{r_p(\theta_{\text{RDS}})}{r_{p0}(\theta_{\text{RDS}})} \right|^2 - \left| \frac{r_s(\theta_{\text{RDS}})}{r_{s0}(\theta_{\text{RDS}})} \right|^2 \right]. \tag{3}$$

Then the relative OIRD intensity is given by

$$\frac{\Delta R}{R_0} = \left[\left| \frac{r_p}{r_{p0}} \right|^2 - \left| \frac{r_s}{r_{s0}} \right|^2 \right]. \tag{4}$$

We monitored the heteroepitaxy of Nb-doped strontium titanate (Nb:STO) (the doping concentration is 10%) on $SrTiO_3$ (STO) (001) in an interrupted growth mode[10] simultaneously by OIRD and RHEED. In the first stage of each growth cycle for this interrupted growth mode, unit cells of about one molecular layer were deposited, then in the interruption time the deposition paused to enable the surface to anneal. Here the pause time is 7 s. The pulses needed for forming one unit-cell layer determined from continuous RHEED oscillations are 36 pulses with the laser pulse repetition of 2 Hz. The substrate temperature obtained from an optical pyrometer is around 660 °C and the oxygen pressure is around 1.0×10^{-4} Pa. Growth conditions with more details have been given elsewhere.[10] With the data acquiring a speed of 0.25 point/s, Fig. 2 shows the interference oscillations obtained by OIRD and the inset shows the oscillations corresponding to the deposition of one unit-cell layer. The thickness corresponding to the interference oscillation period is about 1590 ± 20 Å.

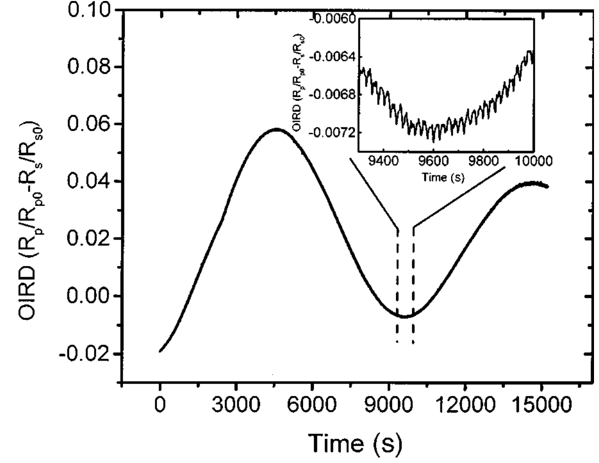

FIG. 2. Interference oscillations and monolayer oscillations (the inset) obtained by OIRD during the heteroepitaxy of Nb-doped $SrTiO_3$ on $SrTiO_3$ (100).

During another deposition process with a longer pause time (>50 s), the OIRD measurement and RHEED measurement were carried out simultaneously. A higher OIRD data acquiring speed (4 points/s) was chosen in order to get more details about the optical response. The detailed monolayer OIRD oscillations are shown in Fig. 3. Figure 3(b) shows the intensity oscillation of the RHEED specular spot, and Fig. 3(c) depicts the OIRD response with arrows indicating the starting and the pausing of each growth cycle. In Fig. 3(b), the RHEED intensity decreases directly when deposition starts, and reaches a minimum value at about a half layer deposition, then it keeps increasing until reaching a maximum where deposition pauses. The RHEED oscillations indicate that the current growth proceeds in a good layer-by-layer growth mode. A sharp peak appears downwards within the OIRD response for the first several deposition pulses. Then the OIRD intensity increases till a maximum and decreases after that. It is noticeable that the maximum of the OIRD intensity comes out a little bit later than the minimum of the RHEED intensity does. The contour of the OIRD curve goes up, which is consistent with the fact that this part is adapted from the ascending part of the interference oscillations. The relative amplitude of the monolayer OIRD oscillations $\Delta R/R_0$ is about $0.5-1\times10^{-3}$ while the interference oscillation amplitude is about 6–9%.

By rotating the substrate along its normal axis ([001] axis) to different angles away from the initial direction, different OIRD responses were measured. The shapes and the amplitudes of the OIRD oscillations did not change significantly, which shows that the OIRD is not so sensitive to the in-plane orientation of the substrate as conventional RDS.

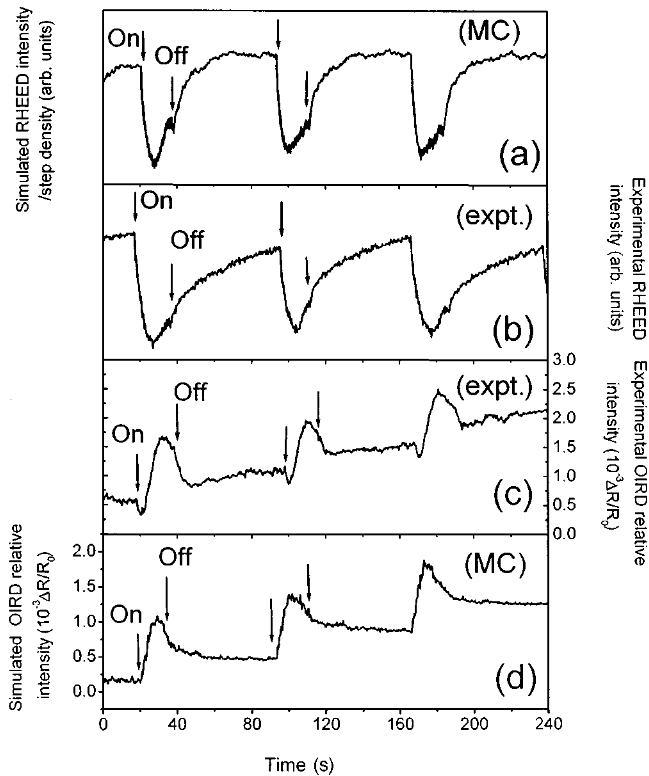

FIG. 3. Detailed OIRD response.(a) simulated RHEED intensity (step density) oscillations given by Monte Carlo (MC) simulation, (b) experimental RHEED intensity oscillations (expt.), (c) experimental OIRD signal, (d) OIRD response given by MC. The noisy pattern in the simulated curve is caused by the dynamic random diffusion of surface units (see text).

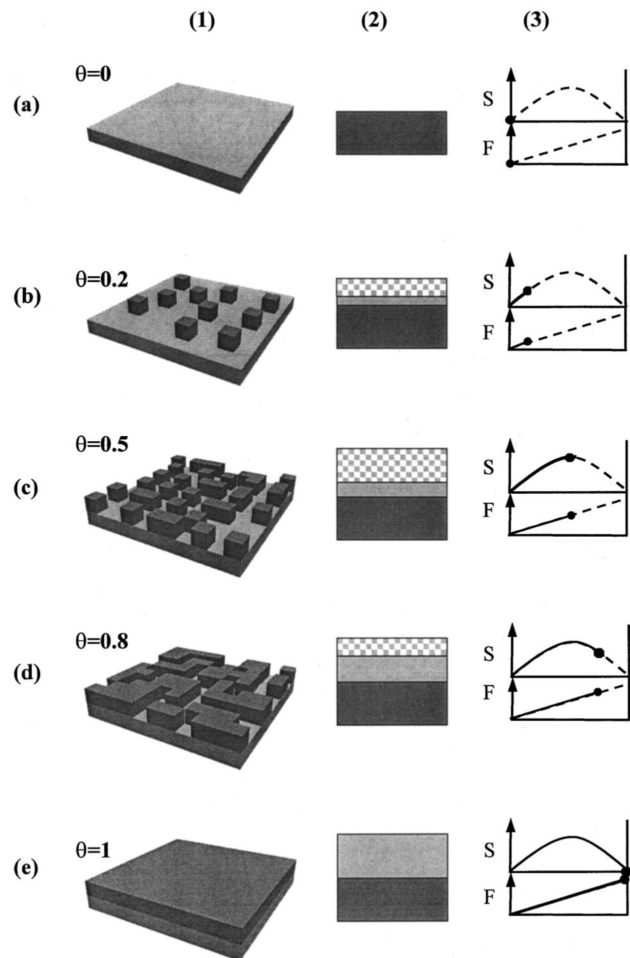

FIG. 5. Schematic representation of the surface morphology for different coverage (column 1), corresponding surface structures (column 2), and variations of the height of surface layer (S) and film thickness (F) (column 3). The dashed curve in column 3 shows the trend of the variations and the solid dot at the end of the solid curve indicates the current value corresponding to the surface morphology shown in column 1.

THEORETICAL MODEL AND NUMERICAL SIMULATIONS

In attempting to model the surface structure to calculate the OIRD response, we treat the topmost incomplete layer as two parts as shown in Fig. 4, a surface layer with an average dielectric constant and a film layer below that with the dielectric constant of the bulk film. To simplify the calculation, we define the dielectric constant of the surface layer as being independent of the surface changes and we treat the surface changes as the variations of the surface layer height. This kind of treatment is similar to that described in Refs. 5 and 6 by Dietz, which is successful in calculating PRS signals. As shown in Fig. 3(c), the relative change of the OIRD signal reaches a maximum value at about half layer coverage (the minimum of the RHEED intensity) which a corresponds to the maximum surface roughness. Thus, in our model, the height of the surface layer is also a maximum value for half layer coverage, smaller for lower or higher coverage. The variations of the surface layer height during layer-by-layer growth are schematically illustrated in Figs. 5(a)–5(e). Column 1 of Fig. 5 shows the schematic surface morphology for different surface coverage θ, column 2 shows the corresponding layer structure in our model. The variations of the surface layer height (S) and the film thickness (F) are shown in column 3. The dashed curve in column 3 shows the trend of the variations and the solid dot at the end of the solid curve indicates the current value corresponding to the surface morphology shown in column 1. At the beginning of the deposition on smooth surface, the surface layer height increases as a result of surface roughening [Figs. 5(a)–5(b)] and reaches a maximum at about half layer coverage [Fig. 5(c)]. During the subsequent growth, the coalescence of two-dimensional (2D) islands, which leads to surface smoothening, results in the corresponding decrease of the height of the surface layer [Figs. 5(d)–5(e)]. The thickness of the bulk film increases continuously throughout the deposition process.

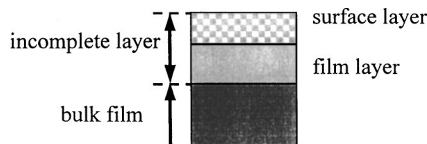

FIG. 4. Schematic illustration of the surface structure in the OIRD model.

Then the surface structure can be described as a four-layer (ambient/surface layer/bulk film/substrate) stack as schematically shown in Fig. 6. When the probe light beam is incident

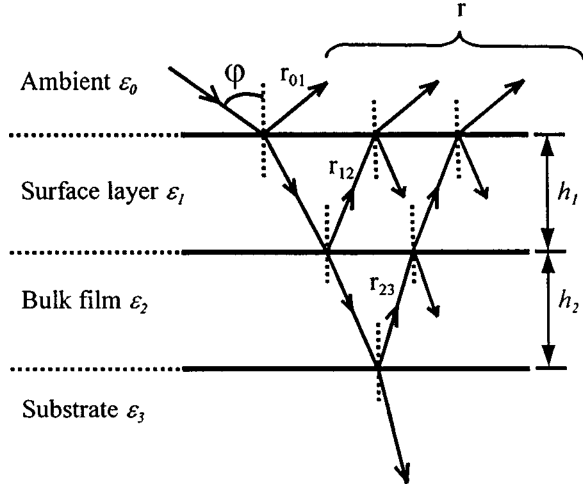

FIG. 6. Schematic representation of a four-layer stack and the multiple reflections of the probe light beam from this stack.

on this four-layer stack, there are multiple reflections at the interfaces between two layers (Fig. 6). A series of beams are reflected back to the ambient. Fresnel's equations for a multilayer stack as described previously[11] are used to calculate the reflectivity of s and p polarization. By numbering the four-layer stack with "0" for ambient, "1" for the surface layer, "2" for the bulk film layer, "3" for the substrate, the complex dielectric constant of each layer can be denoted as $\varepsilon_k(k=0,1,2,3)$. The thickness of the surface layer and the film layer is denoted as h_1 and h_2, respectively. The p-polarized reflection coefficient at the interface between layers k and $k+1$ (from layer k to layer $k+1$) $r^p_{k,k+1}$ is given by[11]

$$r^p_{k,k+1}=\frac{\varepsilon_{k+1}\sqrt{\varepsilon_k-\varepsilon_0\sin^2\varphi}-\varepsilon_k\sqrt{\varepsilon_{k+1}-\varepsilon_0\sin^2\varphi}}{\varepsilon_{k+1}\sqrt{\varepsilon_k-\varepsilon_0\sin^2\varphi}+\varepsilon_k\sqrt{\varepsilon_{k+1}-\varepsilon_0\sin^2\varphi}}. \quad (5)$$

In the same way, we rewrite Fresnel's equation for s polarization with dielectric constant and get

$$r^s_{k,k+1}=\frac{\sqrt{\varepsilon_k-\varepsilon_0\sin^2\varphi}-\sqrt{\varepsilon_{k+1}-\varepsilon_0\sin^2\varphi}}{\sqrt{\varepsilon_k-\varepsilon_0\sin^2\varphi}+\sqrt{\varepsilon_{k+1}-\varepsilon_0\sin^2\varphi}},(k\geqslant 0), \quad (6)$$

where φ is the incidence angle from the ambient. With consideration of the interference effects of all the reflection beams from each layer as shown in Fig. 6, the total reflectance coefficient can be expressed in terms of $r_{k,k+1}$ as[11]

$$r=\frac{r_{0,1}+r_{1,2}e^{-2i\phi_1}+r_{2,3}e^{-2i(\phi_1+\phi_2)}+r_{0,1}r_{1,2}r_{2,3}e^{-2i\phi_2}}{1+r_{0,1}r_{1,2}e^{-2i\phi_1}+r_{0,1}r_{2,3}e^{-2i(\phi_1+\phi_2)}+r_{1,2}r_{2,3}e^{-2i\phi_2}}, \quad (7)$$

where phase factors

$$\phi_1=\frac{2\pi h_1}{\lambda}\sqrt{\varepsilon_1-\varepsilon_0\sin^2\varphi},\quad \phi_2=\frac{2\pi h_2}{\lambda}\sqrt{\varepsilon_2-\varepsilon_0\sin^2\varphi}. \quad (8)$$

$\lambda=6328$ Å is the wavelength in vacuum. By replacing $r_{k,k+1}$ with $r^p_{k,k+1}$ and $r^s_{k,k+1}$ respectively, in Eq. (7), the total reflectance coefficient of p- and s-polarized component r^p and r^s are available. The reflection from the initial surface is simple reflection from a single interface (ambient/substrate interface), the reflectance coefficient r^{p0} and r^{s0} are given by

$$r^{p0}=\frac{\varepsilon_3\cos\varphi-\sqrt{\varepsilon_0}\sqrt{\varepsilon_3-\varepsilon_0\sin^2\varphi}}{\varepsilon_3\cos\varphi+\sqrt{\varepsilon_0}\sqrt{\varepsilon_3-\varepsilon_0\sin^2\varphi}}, \quad (9)$$

$$r^{s0}=\frac{\sqrt{\varepsilon_0}\cos\varphi-\sqrt{\varepsilon_3-\varepsilon_0\sin^2\varphi}}{\sqrt{\varepsilon_0}\cos\varphi+\sqrt{\varepsilon_3-\varepsilon_0\sin^2\varphi}}, \quad (10)$$

respectively.

The complex refractive index of STO substrate at 6328 Å is $\tilde{n}_3=(2.38,0.01)$ determined by McKee *et al.*[12] As the Nb:STO film thickness, h_2 at any time can be determined by RHEED oscillations, the real part n_2 of the complex refractive index $[\tilde{n}_2=(n_2,n_2')]$ of Nb:STO film can be calculated from the interference oscillation period Δh_2. As described in *Principles of Optics* by M. Born,[13] the interference oscillation period corresponds to the change of the thickness of the film

$$\Delta h_2=\frac{\lambda}{2\tilde{n}_2\cos\theta_2}, \quad (11)$$

where θ_2 is the refraction angle determined by $\tilde{n}_0\sin\theta_0=\tilde{n}_2\sin\theta_2$, n_0 is the refractive index of the ambient, and θ_0 is the incidence angle. From Eq. (11), n_2 is calculated to be about 2.25. The imaginary part n_2' of the complex refraction index $\tilde{n}_2$ can be estimated from the damping speed of the amplitude of the interference oscillations. It turns out to be 0.1. The refractive index of the surface layer is approximately taken as $\tilde{n}_1=(1.6,0.35)$. Thus ε_k is simply given by $\varepsilon_k=(\tilde{n}_k)^2$ (we assume $\mu_k=1$). The maximum height is taken as 8 Å with the consideration that the first layer is only 63% covered while the layer above is 31% covered in a simulation of deposition with no diffusions. It is assumed here that the first two layers with the height of 8 Å mainly contribute to the surface layer.

The growth corresponding to the data shown in Fig. 2 is a typical Stranski-Krastanow[14] mode growth as the RHEED intensity damps out quickly for continuous deposition. The growth process is interrupted after about each unit layer deposition to allow the surface morphology to recover.[10] The deposition results in surface roughening while the interruption leads to the recovery of the surface flatness associated with increase in the mean terrace width or reduction of step density.[15] This process can be described by the increase of the surface layer height during the deposition and the subsequent decrease during the interruption. The film thickness keeps on increasing during the deposition and interruption. The variations in one growth cycle can be simply described as

$$h_1=\begin{cases}\dfrac{8t}{T_1},(0\leqslant t\leqslant T_1)\\[2ex]\dfrac{8(t-T_1)}{T-T_1},(T_1\leqslant t\leqslant T)\end{cases}, \quad (12)$$

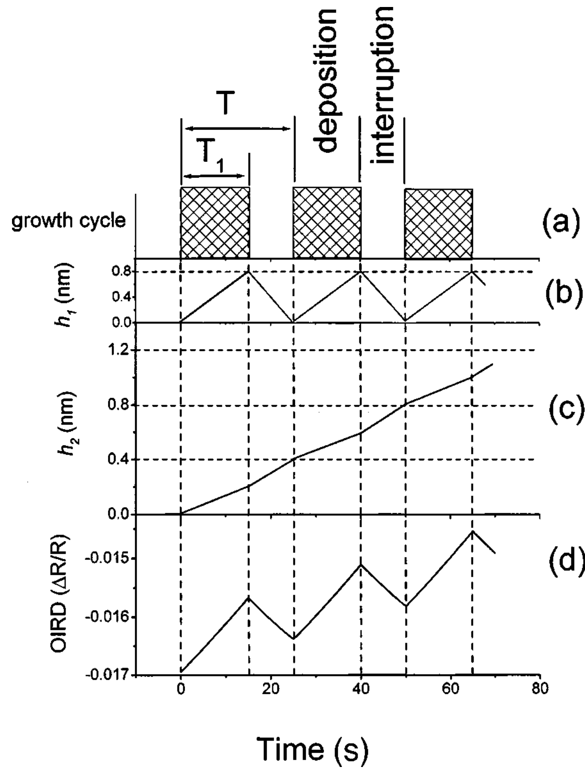

FIG. 7. Growth cycle (a), variations of the surface layer height h_1 (b), film thickness h_2 (c) and the calculated OIRD relative intensity (d) during numerical simulation. T_1 and T are the same as that defined in Eq. (12).

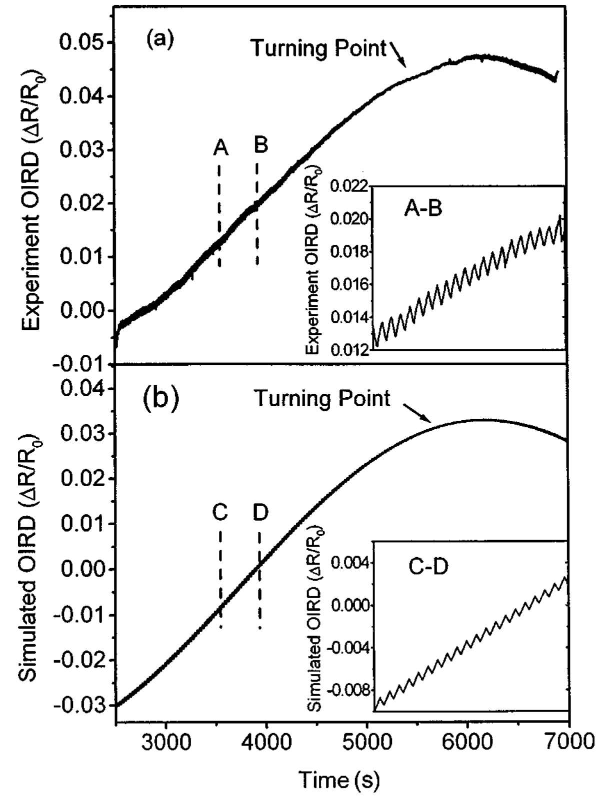

FIG. 8. The OIRD response in (a) experimental results and (b) numerical simulated results. The inset of each shows the monolayer oscillations. The arrow in each figure indicates the turning point.

$$h_2=H_0+\begin{cases}\dfrac{2t}{T_1},(0\leqslant t\leqslant T_1)\\ 2+\dfrac{2(t-T_1)}{T-T_1},(T_1\leqslant t\leqslant T)\end{cases},$$

where $T=25$ s is the growth cycle period, $T_1=18$ s is the deposition time, H_0 is the thin-film thickness after the last growth cycle, which are schematically shown in Figs. 7(a)–7(c) with the simulated OIRD response shown in Fig. 7(d). Figure 8(b) is the numerical simulated curve with the monolayer oscillations shown in the inset. To compare with the simulated curve, the experimental curve (it is another curve different from that shown in Fig. 2) is shown in Fig. 8(a). The amplitude of the simulated interference oscillations is about 6–8 % while that of the monolayer oscillations is about $1-2\times10^{-3}$, which are in agreement with the experimental results at the order of magnitude. In the experiment curve [Fig. 8(a)], there is a so-called turning point as indicated by the arrow, across which the sign of the OIRD response changes. The turning point is similar to that in PRS, which has been discussed by Dietz and co-workers.[5,6] The turning point also occurs in the simulated curve.

MONTE CARLO SIMULATION

To get a better understanding of the optical response and RHEED intensity oscillations shown in Figs. 3(c) and 3(b), basic Monte Carlo simulation[16] (MC) is carried out. The unit cell is treated as a cubic growth unit, whose mobility and the nearest-neighbor bonding of units are isotropic (the solid-on-solid model).[17] The simulations are carried out on a 60×60 flat lattice with periodic boundary conditions. The growth kinetics is described as two processes: the deposition of units onto the substrate at random sites and subsequent migration of surface units. According to the nature of pulsed laser deposition, unit cells are assumed to impinge onto the substrate surface batch by batch (of many units) rather than one by one (unit).[18] The migration is taken as a nearest-neighbor hopping process with the rate $k(T)=k_0\exp(-E_D/k_BT)$, where T is the substrate temperature, $k_0=2k_BT/h$, k_B is Boltzmann's constant, h is Planck's constant, and E_D is the hopping barrier. The hopping barrier of a unit with n lateral nearest neighbors is given by $E_D=E_S+nE_N$, where E_S is the contribution from the unit below the migrating one, E_N is the contribution from each nearest neighbor, $n=0,...,4$. While no accurate value of E_S and E_N have been reported, we take E_S and E_N as 1.1 and 0.05 eV (the error of the absolute value does not change the qualitative results), respectively.

Monte Carlo simulation has shown that surface step density can reproduce the RHEED specular intensity qualitatively[18,19] and quantitatively.[20] The surface step density at the azimuthal angle ϕ ($\phi=0$ at the [110] direction) is given by[19]

$$S=\frac{1}{L}\sum_{i,j}\{[1-\delta(h_{i,j},h_{i+1,j})]\cos\phi+[1-\delta(h_{i,j},h_{i,j+1})]\sin\phi\},\qquad(13)$$

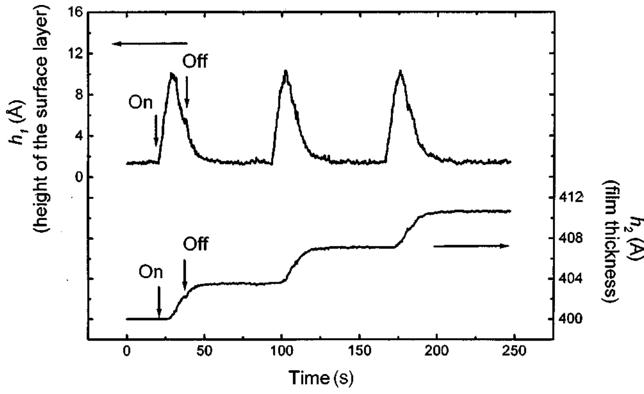

FIG. 9. Variations of the surface layer height (upper curve) and the film thickness (lower curve) obtained by the MC simulations.

where L is the number of the lattice sites, $h_{i,j}$ is the height of the column of units at the lattice site (i, j), and $\delta(a,b)$ is the Kronecker δ function.

To calculate the OIRD signal, one has to determine the height of the surface layer from the surface morphology. Using the number of units in the terrace to represent the terrace area, we find out all those relative large terraces whose areas are larger than 80 unit cells. The total area $S_{\rm total}$ of these ''large'' terraces is obtained by adding up each terrace area. We define the layer mainly deposited during the current growth cycle as ''current layer.'' The areas of those ''large'' terraces of the current layer are summed up and denoted by $S_{\rm curlayer}$. By denoting the total area of the surface with $S_{\rm surface}$ (i.e., 3600) the surface layer height h_1 and film thickness h_2 are given by

$$h_1(\text{Å}) = \left(1 - \frac{S_{\rm total}}{S_{\rm surface}}\right) H_{\rm max}, \quad h_2(\text{Å}) = h_0 + \frac{S_{\rm curlayer}}{S_{\rm surface}} 4, \tag{14}$$

where h_0 is the film thickness after last growth cycle, and $H_{\rm max}$ is a constant that gives the range of the surface layer height.

With $H_{\rm max}=1.2\,{\rm nm}$, $h_0=40\,{\rm nm}$, $T=660\,°C$, 36 pulses needed for depositing one unit-cell layer, laser pulse repetition of 2 Hz, the variations of the surface layer height and film thickness as presented in Eq. (14) are shown in Fig. 9. For the convenience of comparing the simulated curve with the experimental one, the OIRD responses are shown in Fig. 3(d). Corresponding simulate RHEED intensity/step density ($\phi=45°$ for [010] direction) are shown in Fig. 3(a). The noisy patterns in Figs. 3(a), 3(d), and 9 are caused by the dynamic random diffusion and coalescence of the surface units as a nature of the MC method. The simulated RHEED intensity reproduces well the experimental curve [Fig. 3(b)] except the recovery.[19] The quantitative behavior of the recovery, which is not the main features we studied here, has been discussed and solved by Šmilauer.[20] The simulated OIRD curve also reproduces well the main feature of the experimental one except for the absence of the sharp decrease in the simulation curve. The simulated OIRD intensity goes up when the deposition starts, and recovers as it does in the experimental curve. The base intensity after the recovery of the simulated intensity is higher than the initial one as an evidence of the increase of film thickness shown in Fig. 9. The amplitude of the simulated curve is about 6×10^{-4}, which is in good agreement with that of the experiment curve (8×10^{-4}).

DISCUSSION AND CONCLUSIONS

The interference oscillations and monolayer oscillations have been observed during the heteroepitaxy of Nb:STO on STO by OIRD. The interference oscillation is caused by the interference between the reflected light from the surface and that from the film/substrate interface. The period of the interference oscillations can be used for real-time thin-film thickness monitoring. The monolayer OIRD oscillations are verified by simultaneously measured RHEED intensity oscillations, which reveal the layer-by-layer growth of thin films.

The numerical simulation results from the four-layer stack model are in good agreement with the experimental results. The simulated monolayer OIRD oscillations obtained by MC simulation reproduce well the optical response. The agreement between the theoretical results and the experimental results shows that the four-layer stack model is very successful in describing the heteroepitaxy of Nb:STO on STO.

The surface layer in PRS (Refs. 5, 6) is a real layer with different composition and structure from that of the bulk film layer. The surface layer in our model is taken from the outermost incomplete layer by considering it to be an isotropic media layer with an average dielectric constant. Thus the OIRD signal is considered to reveal the changes of the outermost layer and so on to reveal the surface roughness and morphologies.

Our experimental results and theoretical simulations show that OIRD takes the potentiality of monitoring the surface morphologies and roughness for thin-film growth. Thus OIRD may become a good assistant of conventional RHEED for real-time surface monitoring. Further study may make it possible for this technique to give more information about thin-film growth processes and growth mechanisms.

ACKNOWLEDGMENTS

We gratefully acknowledge support from the Ministry for Science and Technology of China.

*Electronic address: yanggz@aphy.iphy.ac.cn

[1] D. E. Aspnes, W. E. Quinn, and S. Gregory, Appl. Phys. Lett. **57**, 2707 (1990); J.-T. Zettler, T. Wethkamp, M. Zorn, M. Pristovsek, C. Meyne, K. Ploska, and W. Richter, *ibid.* **67**, 3783 (1995); K. K. Svitashev, V. A. Shvets, A. S. Mardezhov, S. A. Dvoretsky, Yu. G. Sidorov, N. N. Mikhailov, E. V. Spesivtsev, and S. V. Rychlitsky, Mater. Sci. Eng., B **44**, 164 (1997).

[2] D. E. Aspnes, J. P. Harbison, A. A. Studna, and L. T. Florez, Phys. Rev. Lett. **59**, 1687 (1987); J. P. Harbison, D. E. Aspnes, A. A. Studna, L. T. Florez, and M. K. Kelly, Appl. Phys. Lett. **52**, 2046 (1988); T. Yasuda, K. Kimura, S. Miwa, L. H. Kuo, C. G. Jin, K. Tanaka, and T. Yao, Phys. Rev. Lett. **77**, 326 (1996).

[3] Tat-Kun Kwok and Z. Yang, Appl. Phys. Lett. **80**, 4621 (1996).

[4] J.-T. Zettler, J. Rumberget, K. Ploska, K. Stahrenberg, M. Pristovsek, W. Richter, M. Wassermeier, P. Schützendube, J. Behrend, and L. Däweritz, Phys. Status Solidi A **152**, 35 (1995); C.

C. Kim, Y. P. Chen, M. Daraselia, S. Sivananthan, S.-C. Y. Tsen, and David J. Smith, J. Cryst. Growth **175/176**, 328 (1997).

[5] Klaus J. Bachmann, Uwe Rossow, and Nikolaus Dietz, Mater. Sci. Eng., B **35**, 472 (1995); Nikolaus Dietz and Klaus J. Bachmann, Vacuum **47**, 133 (1996); N. Dietz, U. Rossow, D. E. Aspnes, and K. J. Bachmann, J. Cryst. Growth **164**, 34 (1996).

[6] N. Dietz, N. Sukidi, C. Harris, and K. J. Bachmann, J. Vac. Sci. Technol. A **15**, 807 (1997).

[7] A. J. Pidduck, D. J. Robbins, A. G. Cullis, D. B. Gasson, and J. L. Glaser, J. Electrochem. Soc. **136**, 3083 (1989); A. R. Boyd, T. B. Joyce, and R. Beanland, J. Cryst. Growth **164**, 51 (1996).

[8] X. D. Zhu, H. B. Lu, Guo-Zhen Yang, Zhi-Yuan Li, Ben-Yuan Gu, and Dao-Zhong Zhang, Phys. Rev. B **57**, 2514 (1998).

[9] X.-D. Xiao, Yuanlin Xie, and Y. R. Shen, Surf. Sci. **271**, 295 (1992); A. Wong and X. D. Zhu, Appl. Phys. A: Mater. Sci. Process. **63**, 1 (1996).

[10] Yang Guozhen, Lu Huibin, Wang Hui-sheng, Cui Da-fu, Yang Hai-qing, Wang Hua, Zhou Yueliang, and Chen Zheng-hao, Chin. Phys. Lett. **6**, 178 (1997).

[11] N. Dietz, D. J. Stephens, and K. J. Bachmann, in *Diagnostic Techniques for Semiconductor Materials Processing*, edited by O. J. Glembocki, S. W. Pang, F. H. Pollak, G. M. Crean, and G. Larrabee, MRS Symposia Proceedings No. 324 (Materials Research Society, Pittsburgh, 1994), p. 27.

[12] R. A. McKee, F. J. Walker, E. D. Specht, G. E. Jellison, Jr., L.A. Boatners, and J. H. Harding, Phys. Rev. Lett. **72**, 2741 (1994).

[13] M. Born and E. Wolf, *Principles of Optics*, 6th ed. (Pergamon, Oxford, 1980), pp. 61–66.

[14] D. J. Eaglesham and M. Cerullo, Phys. Rev. Lett. **64**, 1943 (1990); I. N. Stranski and Von L. Krastanow, Akad. Wiss. Lit. Mainz Abh. Math. Naturwiss. Kl. **146**, 797 (1939).

[15] J. H. Neave, B. A. Joyce, P. J. Dobson, and N. Norton, Appl. Phys. A: Solids Surf. **31**, 1 (1983); B. F. Lewis, F. J. Grunthaner, A. Madhukar, T. C. Lee, and R. Fernandez, J. Vac. Sci. Technol. B **3**, 1317 (1985).

[16] S. Clarke and D. D. Vvedensky, Phys. Rev. Lett. **58**, 2235 (1987).

[17] J. D. Weeks and G. H. Gilmer, Adv. Chem. Phys. **40**, 157 (1979).

[18] Kui-juan Jin, Shao-hua Pan, and Guo-Zhen Yang, Surf. Sci. **380**, 522 (1997); V. S. Achutharaman, N. Chandrasekhar, Orioll T. Valls, and A. M. Goldman, Phys. Rev. B **50**, 8122 (1994).

[19] T. Shitara, D. D. Vvedensky, M. R. Wilby, J. Zhang, J. H. Neave, and B. A. Joyce, Phys. Rev. B **46**, 6815 (1992).

[20] Pavel Šmilauer and D. D. Vvedensky, Phys. Rev. B **48**, 17 603 (1993).